Research paper

First-Principles Study of Li_2CaCdH_6: Insights into Electronic, Structural, Mechanical, Optical, and Gravimetric H_2 capacity

Shah Zeb Ullah[1,2]*, Shujaat Ali Khan[1], Danish Rehman[2], U. Fawad[1], Ishfaq Shah[2], Ahmad Junaid[2], Muneeb ur Rehman[2], Junaid Rehman[1], Muhmmad Kamran[2]

[1] Department of Physics, Kohat University of Science and Technology, Kohat, KP, Pakistan
[2] Department of Physics, Government Postgraduate College Kohat, KP, Pakistan

* *Corresponding author:* shahzebkhan2917@gmail.com, ph420222002@kust.edu.pk

Abstract: Hydride perovskites have gained significant attention for their potential applications in hydrogen storage, a cornerstone of sustainable energy. This work uses Density Functional Theory (DFT) to analyze the structure, mechanical, electronic, optical, and hydrogen storage capability of the dilithium calcium cadmium hexahydride (Li_2CaCdH_6). The investigation of its structural properties indicates that Li_2CaCdH_6 crystallizes in space group #225 (Fm-3m), from its ideal lattice constant and volume calculated. The negative final enthalpy of -2.65 eV/atom confirms the thermodynamic stability of Li_2CaCdH_6. The gravimetric hydrogen storage capacity of Li_2CaCdH_6 was determined to be 3.51 wt.%. Electronic property calculations, including band gap and s, p, d, and f orbital contributions to density of states, suggest that the material is a semiconductor of indirect bandgap (M-G) 1.95 eV calculated by generalized gradient approximation with the Perdew-Burke-Ernzerhof functional (GGA-PBE). Additionally, the research estimated Young's modulus, shear modulus, bulk modulus, Poisson's ratio, Pugh's ratio, and anisotropy for Li_2CaCdH_6, verifying its mechanical stability based on Born's stability criterion (C_{ij}). The positive Cauchy's pressure suggests its ductile behavior. The value of B/G = 3.22 also indicates that the examined material has a ductile nature. The calculated Poisson's ratio of 0.36 indicates a predominantly ionic bonding character. Furthermore, DFT was utilized to predict optical properties that are the dielectric function, reflectivity, refractive index, conductivity, absorption, and energy loss function. The present study explores Li_2CaCdH_6 as a potential hydride perovskite for hydrogen storage applications. Further efforts can also lower the desorption temperature to improve feasibility.

Keywords: Anisotropy; Debye temperature; Hydride-Perovskite; Melting temperature; Mechanical properties

1. Introduction

Energy storage is a critical component of contemporary energy systems, especially as the world gradually shifts from fossil fuels to green energy sources [1-3]. Human energy needs are always rising, and the natural gas, coal, and petroleum resources are used to meet them. As fossil fuels get depleted, their costs rise, prompting the search for alternative energy sources. It is feasible to satisfy routine energy demands using energy generated from renewable sources. The usage of clean energy is rapidly rising while the usage of fossil fuels is being reduced in order to comply with worldwide treaties on carbon dioxide emissions. As a result, the usage of renewable energy sources has been encouraged [4]. Conventional hydrogen storage techniques include compressed gas (350–700 bar), liquid hydrogen at −252.8 °C, and underground storage for large-scale applications. However, these approaches face key challenges such as low volumetric density, high energy consumption for compression and liquefaction, safety risks due to high pressure, and hydrogen losses from boil-off in liquid storage [5, 6]. Various materials, including MOFs, metal hydrides, complex hydrides, and high-entropy alloys (HEAs), have been investigated for solid-state hydrogen storage [7, 8]. Energy storage materials, especially solid-state nanoparticles, improve device efficiency by increasing surface area and facilitating charge transfer. Solid-state materials have revolutionized energy conversion and storage processes [9, 10].

DOI: https://doi.org/10.66173/jenmas.2026.106
Received 23 March 2026, Revised 15 April 2026, Accepted 20 April 2026, Available online 18 May 2026

Hydrogen storage problems restrict the broad use of hydrogen energy, since old approaches are expensive in terms of energy and resources [11]. There is growing interest in perovskite hydride materials for hydrogen storage that is critical for developing sustainable energy systems. This interest originates from the necessity for effective hydrogen storage options to support renewable energy technologies [12]. Perovskite-type structures hold immense promise for advancing hydrogen storage technologies and solar cell applications, establishing a robust foundation for future breakthroughs in these critical areas [13].

As attainable compounds for hydrogen storage, potassium manganese trihydride ($KMnH_3$) has a gravimetric hydrogen storage capability of 3.021 wt.% while potassium iron trihydride ($KFeH_3$) has a capacity of 2.994 wt.% [14]. The novel tin-based perovskite hydrides ($XSnH_3$), wherein X refers to rubidium, cesium, and francium, are being explored with a focus on possible uses as hydrogen storage units of 1.45 wt.%, 1.18 wt.%, and 0.87 wt.%, respectively [15]. With gravimetric capacities of 3.771, 3.606, and 3.643 wt.%, respectively, perovskite hydrides, particularly manganese-based $MgXH_3$ (X = Cr, Fe, Mn), demonstrate encouraging hydrogen storage characteristics, rendering them prospective contenders for use in renewable energy storage mechanisms for hydrogen [16]. Lanthanum Chromite ($LaCrO_3$), an oxide perovskite, has shown potential as a hydrogen storage material with a capacity of around 4 wt.% [17]. Conventional intermetallic alloys are unable to achieve the hydrogen storage capacity for desired outcomes [18]. One of the most essential demands for automobiles is hydrogen energy, which is 100% renewable and environmentally friendly [19]. Finding the sweet spot between gravimetric and volumetric densities, while limiting the massive amount of hydrogen gas, is the challenge of hydrogen storage [20]. But advanced solid-state materials are required to achieve the U.S. Department of Energy (DOE) targets for high-capacity, reversible, and energy-efficient onboard storage [21]. Because of its widespread use in metal hydrides and other modified materials, lithium is an important component in hydrogen storage systems. The solid-state uses of Li-based compounds are supported by research that shows they have potential hydrogen storage capabilities [22-24]. Calcium (Ca) has a significant role in hydrogen storage via diversity of compounds and materials, with promising capabilities and stability. Recent research studies encourage calcium's usefulness in improving hydrogen adsorption and storage in various hydride structures making it an appealing constituent in hydrogen storage technologies [25, 26]. However, recent studies indicate that a silver cadmium oxide alloy has been applied in the hydrogen storage device, which possibly contributes to the durability and efficiency of hydrogen storage [27, 28]. Nevertheless, theoretical investigations into the electronic, mechanical, and optical properties of materials remain relatively scarce, despite their critical importance in understanding the interplay between electronic and optical behaviors in double perovskite materials [29].

In this work, the ab-initio calculations are used to scientifically examine the structural, electronic, mechanical, and optical properties of Li_2CaCdH_6, with a specific focus on its potential for hydrogen storage applications. This material was chosen due to its limited prior study and promising characteristics, including high hydrogen capacity, favorable formation energy, and structural and mechanical stability, with the aim of assessing its potential for advanced energy storage applications.

2. Computational Method

DFT is the most suitable approach for nowadays research because it allows for an integrated analysis of its physical properties at the atomic level. The geometry of the hydride perovskite Li_2CaCdH_6 was optimized in DFT calculations using the Cambridge Serial Total Energy Package (CASTEP) [30, 31]. The GGA-PBE approximation was employed due to its proven reliability in describing the ground-state properties of solid-state systems. In hydrogen storage research, this method allows for a detailed atomic-level evaluation of adsorption energies and electronic interactions, providing a fundamental understanding of the bonding mechanisms that govern hydrogen uptake and release. Exchange correlation was treated within the GGA-PBE functional, which underestimates band gaps and van der Waals interactions, but it remains highly efficient for large systems due to its low computational cost and rapid band structure estimation [32-35]. Even though this approximation efficiently predicts the contribution of orbitals in the valence and conduction bands. The electron-ion interactions were defined, retaining the Projector Augmented Wave (PAW) method [36, 37] with a cut-off of 598 eV for kinetic energy. The PAW method, together with Ultrasoft Pseudopotentials (USPP), this specific combination was adopted to guarantee high numerical precision for the Cd-4d states while preserving computational efficiency. The Brillouin zone was sampled using a 4×4×4 Monkhorst-Pack k-point grid [38, 39], and Vanderbilt ultrasoft pseudopotentials [40] were applied for the electron-ion potential. Notably, USPP facilitates a lower plane-wave kinetic energy cut-off without reducing the reliability. Broyden-Fletcher-Goldfarb-Shanno (BFGS) algorithm with Pulay density mixing scheme was used to perform energy minimization [41, 42]. The maximum force was set to 0.03 eV/Å, the

maximum ionic displacement to 0.001 Å, and the total energy/atom to 1.0 $\times 10^{-5}$ eV. Elastic constants were used to evaluate mechanical stability and material properties [43]. Computational and theoretical approximations were employed to systematically evaluate the material's structural stability, mechanical behavior, and optical characteristics. Elastic constants for a cubic crystal structure are C_{11}, C_{12}, and C_{44}. Elastic moduli were determined using the Voigt [44], Reuss [45], and Hill [46] approximations. The Voigt method gives the maximum value of the modulus, the Reuss method provides the minimum value, and the Hill approximation is the arithmetic mean of the two.

$$G = \frac{1}{2}(G_V + G_R) \tag{1a}$$

$$G_V = \frac{1}{5}(C_{11} - C_{12} + 3C_{44}) \tag{1b}$$

$$G_R = \frac{5C_{44}(C_{11} - C_{12})}{4C_{44} + 3(C_{11} - C_{12})} \tag{1c}$$

$$A = \frac{2C_{11}}{C_{11} - C_{12}} \tag{2a}$$

$$Y = \frac{9GB}{3B + G} \tag{2b}$$

$$\nu = \frac{3B - 2G}{2(2B + G)} \tag{2c}$$

G, A, Y, and ν are the shear modulus, anisotropy factor, Young modulus, and Poisson ratio, respectively.

The optical properties can be calculated by using these equations:

$$\varepsilon_1(\omega) = 1 + \frac{2}{\pi} P \int_0^{\infty} \frac{\omega' \varepsilon_2(\omega')}{\omega'^2 - \omega^2} d\omega' \tag{3a}$$

$$\varepsilon_2(\omega) = -\frac{2\omega}{\pi} P \int_0^{\infty} \frac{\varepsilon_1(\omega') - 1}{\omega'^2 - \omega^2} d\omega' \tag{3b}$$

The $\varepsilon_1(\omega)$ and $\varepsilon_2(\omega)$ are the real and imaginary part of dielectric function.

$$\eta(\omega) = \left(\frac{\varepsilon_1(\omega)}{2} + \frac{\sqrt{[\varepsilon_1(\omega)]^2 + [\varepsilon_2(\omega)]^2}}{2}\right)^{1/2} \tag{4a}$$

$$\kappa(\omega) = \left(\frac{\sqrt{[\varepsilon_1(\omega)]^2 + [\varepsilon_2(\omega)]^2}}{2} - \frac{\varepsilon_1(\omega)}{2}\right)^{1/2} \tag{4b}$$

The above eq. 4a and 4b are the real (Re) η(ω) and imaginary (Im) κ(ω) components of refractive index.

$$R(\omega) = \frac{n + ik - 1}{n + ik + 1} \tag{5}$$

$$\alpha(\omega) = \frac{4\pi}{\lambda} \kappa(\omega) \tag{6}$$

$$L(\omega) = \mathrm{Im}\,(\varepsilon(\omega)^{-1}) = \frac{\varepsilon_2(\omega)}{\varepsilon_2{}^2(\omega)} + \varepsilon_2{}^2(\omega) \tag{7}$$

The eq. 5, 6, and 7 for the reflectivity, absorption coefficient, and loss function correspondingly.

3. Results and Discussion

3.1 Structural Properties

Figure 1 depicts the face-centered cubic crystal structure of the double hydride-perovskite Li_2CaCdH_6, which belongs to space group Fm-3m (#225).

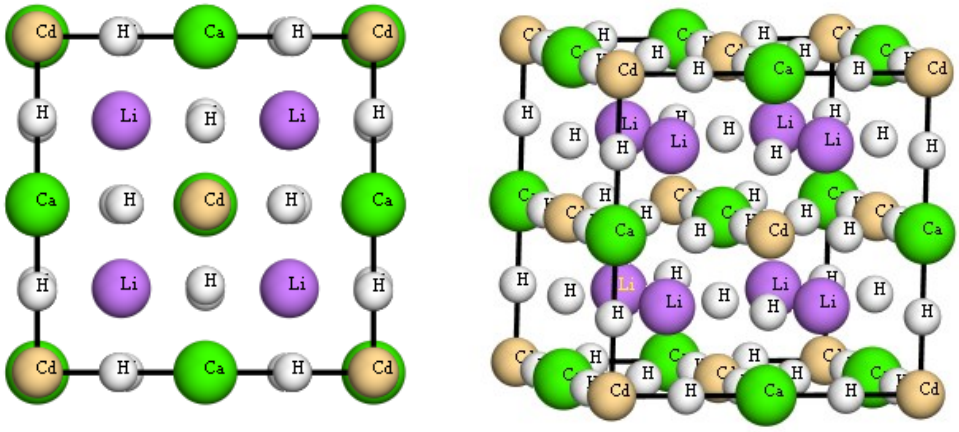

Figure 1. Equilibrium crystal structure of double perovskite Li_2CaCdH_6

During the optimization process of the cubic phase structure of the compound, the Wyckoff positions of the atoms in Li_2CaCdH_6 were detailed in Table 1: Calcium (Ca) atoms were positioned in the center of the unit cell; Cadmium (Cd) atoms were positioned at the; and Hydrogen (H) and Lithium (Li) atoms were situated at coordinates shown in Table 1.

Table 1. Techniques for Material-assisted Microbial Dye Degradation

Element	Wyckoff	x	y	z
Cd	4a	0	0	0
Ca	4b	0.5	0	0
Li	8c	0.25	0.25	0.25
H	24e	0.25	0	0

The optimized lattice constant for the structure was determined to be 8.271 Å, with the corresponding volume of the optimized unit cell calculated as 565.85 $Å^3$. The density of the Li_2CaCdH_6 compound was found to be 2.024 g/cm^3. Additionally, the final enthalpy was calculated by using equation 8, and its negative value strongly indicates the thermodynamic stability of the Li_2CaCdH_6 compound.

$$\Delta H_f = \frac{E_{total}^{Li_2CaCdX_6} - \left[2\,E_{total}^{Li_2} + E_{total}^{Ca} + E_{total}^{Cd} + 6E_{total}^{H_6}\right]}{N} \quad (8)$$

The formation energy per atom (ΔH_f) for the Li_2CaCdH_6 perovskites is calculated using the above relation. Where E_{tot} (Li_2CaCdH_6) is the total energy of the optimized compound, E_{tot}(Li), E_{tot}(Ca), E_{tot}(Cd), and E_{tot}(H) represent the energies of the isolated constituent atoms in the material, and N is the total number of atoms in the unit cell. The total energy of the structure was computed and used to derive key ground-state properties, including the crystal cell volume (lattice constants) and the bulk modulus (B_o) at the minimum equilibrium volume. To fit the premeditated total energies, Birch-Murnaghan's equation of state [39] was employed, utilizing the following expression:

$$E(V) = E(V_o) + \frac{BV}{B'(B'-1)}\left[B\left(1 - \frac{V_o}{V}\right) + \left(\frac{V_o}{V}\right)^{B'}\right] \quad (9)$$

In Equation 9, E(V) corresponds to the energy at a specified volume V, and E(V_o) signifies the total energy of the unit cell at its equilibrium volume V_o. The term B symbolizes the bulk modulus, while B′ refers to the 1st derivative of the bulk modulus with respect to the pressure.

3.2 Hydrogen Storage Capacity

A theoretical equation is applied to estimate the gravimetric hydrogen storage capacity Cwt.% of Li_2CaCdH_6 hydride-perovskite, assessing its viability for hydrogen storage appliances. The Cwt.% metric quantifies the mass of deposited hydrogen relative to the host perovskite's mass, as defined by the following formula [47, 48]:

$$C_{wt.\%} = \left(\frac{\left(\frac{H}{M}\right) m_{Hydrogen}}{m_{Host} + \left(\frac{H}{M}\right) m_{Hydrogen}} \right) \quad 10(a)$$

$$T_{des} = \frac{\Delta H_f}{\Delta S} \quad 10(b)$$

In equation 10a, $m_{Hydrogen}$ represents the hydrogen molar mass, m_{Host} denotes the host compound molar mass, and H/M is the ratio of hydrogen atoms to compound atoms. The $C_{wt.\%}$ values, accessible in Table 2, indicate the hydrogen's gravimetric storage capacity of Li_2CaCdH_6 perovskite. With a $C_{wt.\%}$ value of 3.51, Li_2CaCdH_6 demonstrates significant potential as a capable candidate for hydrogen (H_2) storage applications. Li_2CaCdH_2 demonstrates a hydrogen storage capacity of 3.51 wt.%, achieving 64% of the U.S. DOE's 2025 interim target (5.5 wt.%) and 54% of the ultimate storage goal (6.5 wt.%) [49]. In comparison, this performance places it below the highest-capacity complex hydrides like $LiBH_4$ (18 wt.% theoretical) [50]. In equation 10b, ΔH_f and ΔS are the formation enthalpy and hydrogen entropy, ΔS =130.7 J/mol. K respectively. The compound shows significant advantages over conventional metal hydrides in terms of desorption temperature (at which H_2 release), 938.5 K, which is more moderate than many high-capacity alternatives.

Table 2. Optimized the compounds parameter and compression with Li_2CaCdH_6

Compounds	a (Å)	V (Å^3)	E_g (eV)	λ (nm)	$C_{wt.\%}$	Ref.	
Li_2CaCdH_6	8.27	565.85	1.95	635.82	3.51	This work	theoretical
K_2NaScH_6	8.62	640.503	4.41	281.179	5.08	[52]	theoretical
$NaCaH_3$	4.35	82.312	2.23	563.636	4.38	[51]	theoretical
Ca_2FeH_6	4.87	115.50	1.67	742.514	4.28	[53]	theoretical
K_2LiAlH_6	7.93	498.677	2.82	439.716	3.771	[52]	theoretical
$KCaH_3$	3.92	60.45	2.71	457.56	3.67	[48]	theoretical
Na_2CaCdH_6	8.405	593.764	2.08	596.153	2.956	[12]	theoretical
$KSrH_3$	4.77	108.50	1.41	879.432	2.33	[54]	theoretical
Rb_2CaCdH_6	8.76	674.07	2.30	539.130	1.69	[29]	theoretical

3.3 Electronic Properties

The band structure determines the available energy levels where electrons can exist to control the electrical behavior of compounds. An inspection of the band structure enables materials classification into insulator, semiconductor, and conductor. The electronic band structure calculation of Li_2CaCdH_6 appears in Figure 2a. A horizontal red line marks the Fermi level at 0.0 eV position. The materials framework consists of two energy portions that include the valence band (V.B), lower, and the conduction band (C.B), higher in energy. The band gap of the compound reveals an indirect Band gap (M-G) of 1.95 eV because

valence and conduction bands throughout the structure do not merge together. It confirmed that Li2CaCdH6 shows semiconducting behavior according to its band gap analysis [55].

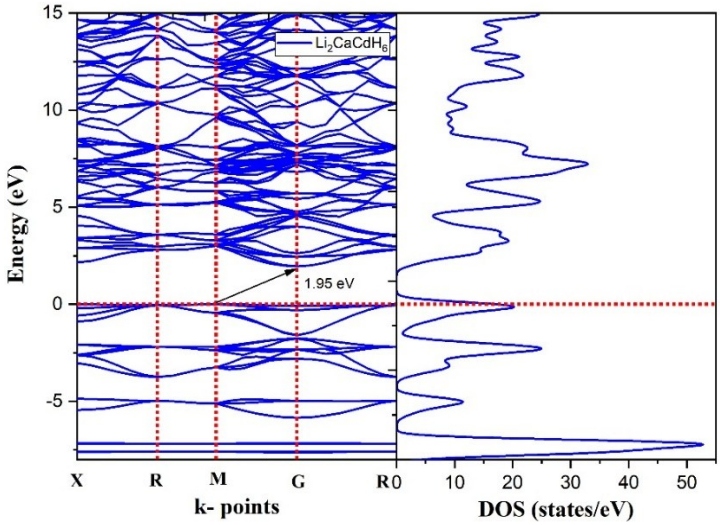

Figure 2. Calculated electronic band structure and total density of states (DOS) of Li_2CaCdH_6

Figure 2 (b) shows the Density of States (DOS) curve that illustrates how individual elements affect the entire band structure. Both bands in Li_2CaCdH_6 reach their maximal density of states at 32.91 states/eV (7.26 eV) in C.B and 52.94 states/eV (-7.21 eV) in V.B., while the Fermi level intersects (20.16 eV/states, -0.11 eV). The C.B contains 2.0 to 4.0 eV occupancy from s-states, but the p-state stands out within 6.0 to 10.0 eV. The C.B contains the d-state and extends from 2.0 eV through 4.0 eV, where multiple states, including d- and p-states, affect both C.B and V.B regions. The majority of s-states and d-states exist in the vicinity of the Fermi level and within the V.B. Both DOS analysis and PDOS analysis of Li_2CaCdH_6 were performed over different energy ranges that extended from (-8 to 8) eV and (-8 to 20) eV, respectively. The PDOS measurement around the Fermi level identifies 20.45 states/eV in Li_2CaCdH_6, together with the separate PDOS values of 3.84 states/eV for Li, 7.99 states/eV for Ca, 3.85 states/eV for Cd, and 5.84 states/eV for H, respectively. The partial density of states for Li_2CaCdH_6 receives major support from the elements H, Li, and Ca. The C.B region shows Li and Ca are the principal elements in figure 3 (a–d) where Li s- and p-orbital peaks are seen at (3.31 eV, 6.19 states/eV) and (7.32 eV, 16.28 states/eV) and Ca exhibits prominent d-orbital peaks at (3.75 eV, 7.70 states/eV) and (7.18 eV, 10.36 states/eV).

In contrast, cadmium (Cd) primarily contributes through its d-orbital in the valence band, with a prominent peak at (-7.28 eV, 52.20 states/eV). The s orbitals and p-orbitals of Cd show minimal contribution, while the f-orbital plays no role. The s-orbital of hydrogen (H) significantly contributes to the valence band, with one of its peaks (-0.10 eV, 14.01 states/eV) crossing the Fermi level and partially contributing to the conduction band's minima. Other peaks for the H-atom are observed at (-2.24 eV, 16.63 states/eV), (-4.99 eV, 7.00 states/eV), and (-7.59 eV, 2.10 states/eV). The red dotted line at 0 eV denotes the Fermi level. The curves collectively indicate that the f-orbital has no contribution to either the DOS or PDOS.

Li_2CaCdH_6 works based on how hydrogen (H), lithium (Li), calcium (Ca), and cadmium (Cd) interact with each other at the orbital level. The main role of the hydrogen 1s orbital is to form the valence band as a hydride ion (H^-) and to bond by ionic and polar covalent methods with lithium (Li^{2+}), calcium (Ca^{2+}), and cadmium (Cd^{+2}). Molecular orbitals of the H-s states are found mostly in the valence band (V.B.), while some also overlap with the conduction band due to weak antibonding effects. The 2s orbital of lithium is closed, which allows it to donate electrons strongly and play a deep role in the C.B., but without much hybridization or ability to conduct electricity. In its Ca^{2+} form, calcium has strong bonds with H^- and uses both its 4s and part of its 3d orbitals in the lower C.B. The covalent bond between cadmium and hydrogen is caused by mixing of the outermost orbitals of cadmium and hydrogen atoms. The weak effect of Cd-d on the V.B. is important to note, while the 5s/p orbitals may be close

to the C.B., but have a very small effect on conductivity. From the overall electron structure, it is clear that the compound acts as a semiconductor, with the valence band having localized H and Cd states, and the conduction band filled by Ca and Li states, and minor H states.

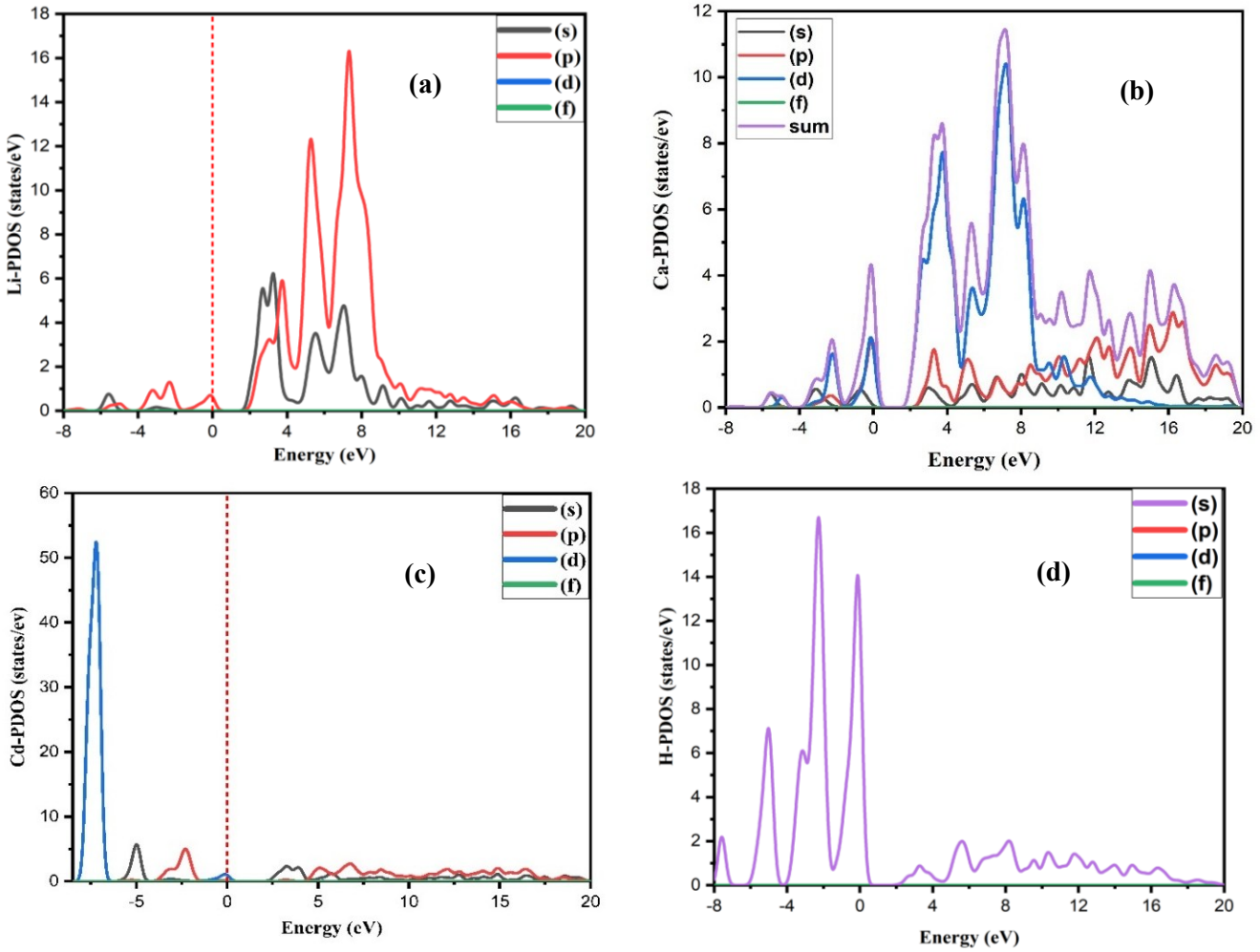

Figure 3. Partial density of states of Li_2CaCdH_6 (**a**) Li- (**b**) Ca- (**c**) Cd- (**d**) H-PDOS.

3.4 Mechanical and Anisotropic Elastic Properties

The material's mechanical stability - and consequently its industrial performance is fully described through its elastic constants (C_{ij}). These constants were calculated using CASTEP. For cubic structures, the essential elastic constants are C_{11}, C_{44}, and C_{12}, which are provided in Table 2 for Li_2CaCdH_6. The estimated values meet the well-established Born stability criteria [56, 57], as given in eq. (11). Consequently, the material is confirmed to be mechanically stable, with $C_{11} - C_{12} = 23.11558$ and $C_{11} + 2C_{12} = 94.75435$, making them suitable for further mechanical property calculations.

$$\begin{matrix} C_{11} > 0; & C_{44} > 0; \\ C_{11} - C_{12} > 0; & C_{11} + 2C_{12} > 0 \end{matrix} \quad (12)$$

The computed elastic constants can be used to derive various physical parameters, like Young's modulus, shear modulus, and bulk modulus, which are accessible in Table 2. The bulk modulus (B) quantifies a material's resistance to volume change under applied pressure. As evident from Table 2, Li_2CaCdH_6 shows the highest bulk modulus of 31.585 GPa. The shear modulus (G), estimated by the ratio of shear-stress to shear-strain, is a critical parameter for assessing hardness, with higher values indicating greater opposition to plastic deformation. In contrast, the bulk modulus (B) reflects the material's opposition to fracture. Young's

modulus (Y) represents the ratio of tensile stress to strain and serves as an important estimate of the material's stiffness. A material having a higher estimate of Young's modulus (E) will be stiffer. These properties collectively provide essential understandings into the mechanical behavior of the compound.

The anisotropy (A) in (eq. 5a) is the degree of elastic anisotropy in cubic crystals, so that A = 1 means consistent isotropy. The studied material has an anisotropy factor of A = 4.07, and that is why the material has an anisotropic nature. Poisson's ratio (ν) in (eq. 5c) indicates, to some extent, the nature of the bonding in the material, as it indicates how much perpendicular expansion or contraction will occur during compression or expansion. The Poisson's ratio of the order of 0.1 might indicate covalent bonding, and 0.25, 0.3 values for ionic bonding. It is found that the studied compound has a Poisson's ratio of 0.36, which confirms that there is a predominant bonding character, which is ionic. Another critical parameter for the brittle or ductile behavior of a material is the B/G ratio (Pugh's modulus). A B/G ratio greater than 1.75 specifies ductility, while a B/G ratio less than this means that the material is brittle, according to Pugh's criterion. The value of B/G = 3.22 indicates that the examined material has a ductile nature. Furthermore, the Cauchy pressure (C_P) = $C_{12} - C_{44}$ is a solid indicator of the material's behavior. A positive C_P value produces ductility; a negative C_P value constitutes brittleness. It is further confirmed that the studied compound has ductile characteristics for the studied compound, as evidenced by the positive C_P values.

Anisotropic elastic properties and the Debye temperature were determined to analyze the material further. The ELATE code was used to create 2D and 3D visualizations [58] of the directional dependence of Young's modulus (Y), shear modulus (G), linear compressibility (β), and Poisson's ratio (υ) at specific conditions for Li_2CaCdH_6, as illustrated in Figure 4. Three-dimensional spherical plots represent isotropy, while non-spherical shapes indicate anisotropy. The 3D contour plots for the studied compound reveal non-spherical shapes, confirming elastic anisotropy in all directions. However, the linear compressibility of the compound is isotropic across all directions [59]. For Li_2CaCdH_6, the parameters E, G, β, and υ exhibited consistent behavior across the xy, yz, and zx planes, further highlighting its anisotropic elastic properties.

Table 3. The computed elastic parameters: [C_{11}, C_{12}, C_{44}] (GPa), Bulk modulus B (GPa), Shear modulus G (GPa), Young's modulus Y (GPa), Poisson's ratio (υ), Pugh ratio (B/G), anisotropy factor (A), and Cauchy pressure (C_P)

Compound	C_{11}	C_{12}	C_{44}	B	G	Y	υ	B/G	A	C_P
Li_2CaCdH_6	46.995	23.879	8.641	31.585	9.808	26.665	0.36	3.22	4.07	15.24

3.4.1 Debye Temperature

The Debye temperature (T_D) is strictly associated with various other properties of a material, including melting temperature and heat capacity. A greater Debye temperature typically implies better thermal conductivity and a higher melting point for the material. The computed values of the velocity of longitudinal-wave (V_l), velocity of transverse-wave (V_t), average wave velocity (V_m), and T_D are presented in Table 4. T_D, V_m, V_l, and V_t were determined by the equations below [60, 61]. In equation (12a), h represents Planck's constant, n (No. of atoms per unit cell), k (Boltzmann constant), ρ (density), M (unit cell atoms mass), and NA (Avogadro's number).

$$T_D = \frac{h}{k}\left[\frac{3n}{4\pi}\left(\frac{N_a\rho}{M}\right)\right]^{1/3} v_m \qquad 12(a)$$

$$v_m = \left[\frac{1}{3}\left(\frac{2}{v_l^3} + \frac{1}{v_t^3}\right)\right]^{-1/3} \qquad 12(b)$$

Utilize the G and B values, to get the values of υ_l and υ_t.

$$v_l = \sqrt{\frac{3B + 4G}{\rho}} \quad \text{and} \quad v_t = \sqrt{\frac{G}{\rho}}. \qquad 12(c)$$

The melting temperature (T_m) has also been calculated by using equation (13) [62].

$$T_m\,(K) = [553(K) + 5.911C_{11}] \pm 300K \quad (13)$$

Table 4. Computed Debye temperatures point (T_D), transverse (υ_t), longitudinal (υ_l), and average (υ_m) wave-velocities and melting points (T_m) for Li_2CaCdH_6

Compound	T_D (K)	υ_t (m/s)	υ_l (m/s)	υ_m (m/s)	T_m (K)
Li_2CaCdH_6	303.20	2021.3	8136.3	2886.0	830.79 ± 300

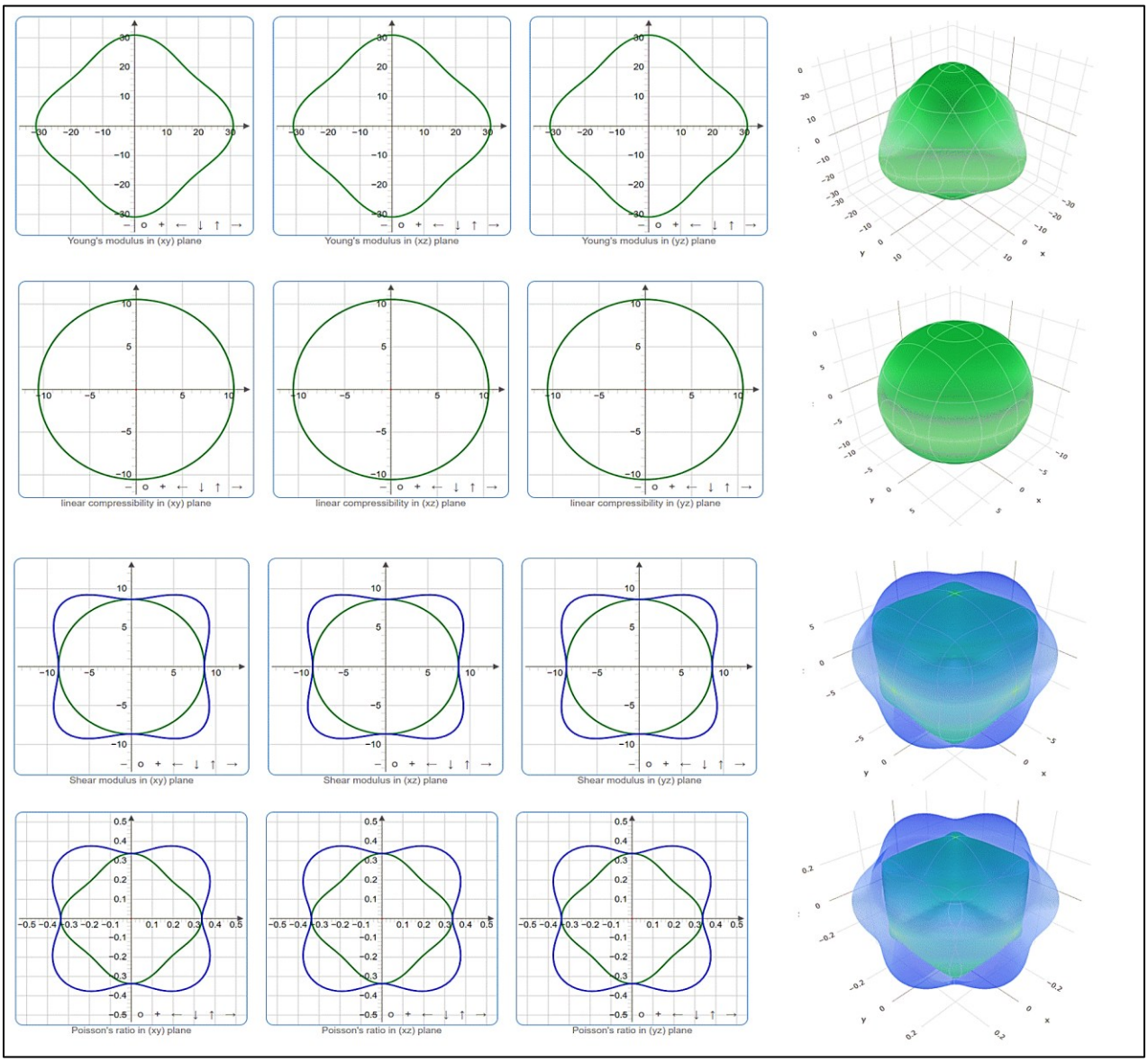

Figure 4. Anisotropy 2D and 3D plots for Li_2CaCdH_6

3.5 Optical Properties

This portion primarily focuses on exploring the material's optical properties to understand their interactions with EM waves (electromagnetic photons). A comprehensive analysis of the optical properties, emphasizing intraband shifts, shows a semiconductor nature, as illustrated in Figure 5 (a-f). Our results align with the well-established Drude model, originally proposed by the renowned scientist Drude [63, 64]. By calculating optical parameters, our intention is to evaluate the potential of the

studied perovskite compound for hydrogen (H_2) storage purposes. The solid material's optical properties can be investigated through their electronic dielectric function, which is largely influenced by intra-band and inter-band transitions, as expressed via Ehrenreich Cohen formulation as $\varepsilon(\omega) = \varepsilon_1(\omega) + i\varepsilon_2(\omega)$ [65]. Here, $\varepsilon(\omega)$ characterizes the interaction of material with EM waves and is divided into two components: $\varepsilon_1(\omega)$, which indicates polarization, and $\varepsilon_2(\omega)$, which describes energy dissipation within the system [66]. The real and imaginary components of the dielectric function are denoted as $\varepsilon_1(\omega)$ and $\varepsilon_2(\omega)$, respectively, as depicted in Figure 5a.

The imaginary part of the dielectric function, depending on $(\omega'^2 - \omega^2)$, can be utilized to compute the real portion of the dielectric function. Additionally, ω' is directly related to the energy bandgap (E_g). The real part, $\varepsilon_1(\omega)$, can result from the Kramers-Kronig (KK) relation [67]. Conversely, the Kramers-Kronig relation can also be employed to get the imaginary part from the real component, establishing a fundamental connection between the two parts of the dielectric function.

For the compound Li_2CaCdH_6, the real part of the dielectric function, ε_1 (0), has a value of 4.41. The highest value of $\varepsilon_1(\omega)$ for Li_2CaCdH_6 is 6.27, occurring at 4.29 eV. On the other hand, the imaginary component of the dielectric function, ε_2 (0), begins at 1.18 eV with a value of 0.00. The compound Li_2CaCdH_6 exhibits the highest peak in $\varepsilon_2(\omega)$ at 7.81 eV, with a value of 5.17. Figure 5.b illustrates the refractive index for both the real (Re) $\eta(\omega)$ and imaginary (Im) $\kappa(\omega)$ components. The maximum (Re) $\eta(\omega)$ for Li_2CaCdH_6 is approximately 2.66 at 4.53 eV, while the imaginary component peaks at 1.89 at 6.03 eV. The static η (0) and the imaginary refractive index $\kappa(\omega)$ for Li_2CaCdH_6 are 2.10 and 0, respectively. The real part of the refractive index reaches 2.65, with its highest peak at 4.71 eV. The $\kappa(\omega)$ or extinction coefficient begins at 1.52 eV with a value of 0.01 and attains its maximum peak of 1.82 at 5.61 eV.

Reflectivity measures a material's ability to reflect incoming radiation, providing insights into how light photons interact with its electronic structure. To analyze the frequency-dependent reflectivity $R(\omega)$ of the hydride perovskite against incident radiation energy ranging from 0.00 to 80.00 eV, it is plotted in Figure. 5c. These results offer valuable information about the optical response of the material and its prospective applications in various technologies. At zero energy, the static reflectivity R (0) of the compound is 0.12. The reflectivity peaks at various energies, with the highest peak of 0.35 occurring at 5.94 eV. Other notable reflectivity values include 0.04 at 14.71 eV, 0.01 at 23.81 eV, and 0.05 at 28.07 eV. As the photon energy increases to the high energy values, the reflectance decreases sharply to a minimum value of 0.00 at 39.79 eV. Conversely, the highest absorption for Li_2CaCdH_6 was observed in this high-energy region.

The research also utilized conductivity $\sigma(\omega)$ to analyze how electrons (incident) interact with the surface of Li_2CaCdH_6 hydride perovskites, leading to bond breaking and conduction due to the photoelectric effect. Figure. 5d presents the frequency-dependent conductivity of Li_2CaCdH_6 hydride-perovskite in the energy range from 0.0 to 80.0 eV, revealing the influence of incoming photon energy on the real (Re) part of $\sigma(\omega)$. Li_2CaCdH_6 exhibited the maximum conductivity of 4.86 (1/fs) at 5.47 eV. The optical investigation suggests that Li_2CaCdH_6 is a promising candidate for hydrogen storage applications, due to its notable conductivity at specific photon energies. The imaginary component of the compound's conductivity peaks at -2.76 (1/fs) at 4.52 eV.

The absorption coefficient $\alpha(\omega)$ plays a crucial part in finding the length to which light travels in a material. It depends on the wavelength (or energy, $E=hc/\lambda$) of the incident photons. Materials with high absorption coefficients tend to absorb photons more rapidly, exciting electrons into the conduction band. Figure. 5e presents the calculated absorption coefficients for the perovskite Li_2CaCdH_6, mapped against incoming photon energy, from 0.0 to 80.0 eV. Notably, the studied material exhibited no absorption $\alpha(0)$ [68]**.** The study highlights a significant and sudden surge in the absorption of Li_2CaCdH_6 as the incident energy rises. The highest absorption for the compound in the ultraviolet region reaches 169,247.33 cm^{-1} at 5.89 eV, as depicted in the graphs. At higher frequencies, the absorption coefficients for all materials examined were found to be nearly zero. Additional absorption peaks were observed at 108,870.97 cm^{-1} (23.94 eV), 167,849.46 cm^{-1} (27.38 eV), and 106,612.90 cm^{-1} (55.19 eV).

The loss-function $L(\omega)$, which represents the energy lost by electrons during transitions due to dispersion or scattering, is directly proportional to the inner shell transitions scattering probabilities. Figure. 5f illustrates the loss function of Li_2CaCdH_6 plotted against incident energy, ranging from 0.0 to 80.0 eV. The graph indicates that the loss function remains at 0.00 until the photon energy reaches 1.80 eV, after which distinct peaks are observed. Likewise, the curve reveals a maximum spike top at 2.10 for radiation energy of 11.20 eV. Similarly, other notable peaks include 0.54 at 24.33 eV, 1.07 at 28.70 eV, and 0.26 at 55.19 eV. The sharp decline in the loss function at higher energies for the examined Li_2CaCdH_6 is expectedly attributed to plasmon

emission. The results suggest that Li_2CaCdH_6 is a promising candidate for efficient EM wave absorption, as it exhibits no energy loss by the electrons in the infrared range and has the least energy L(ω) in the visible range. The release of photoelectrons occurs when E = ħω photons interact with the material's surface. This interaction underscores the potential of Li_2CaCdH_6 in applications requiring effective photon absorption and energy conversion. These findings indicate the potential for photochemical activation of hydrogen storage processes, which could replace conventional thermal methods and significantly reduce energy requirements [69].

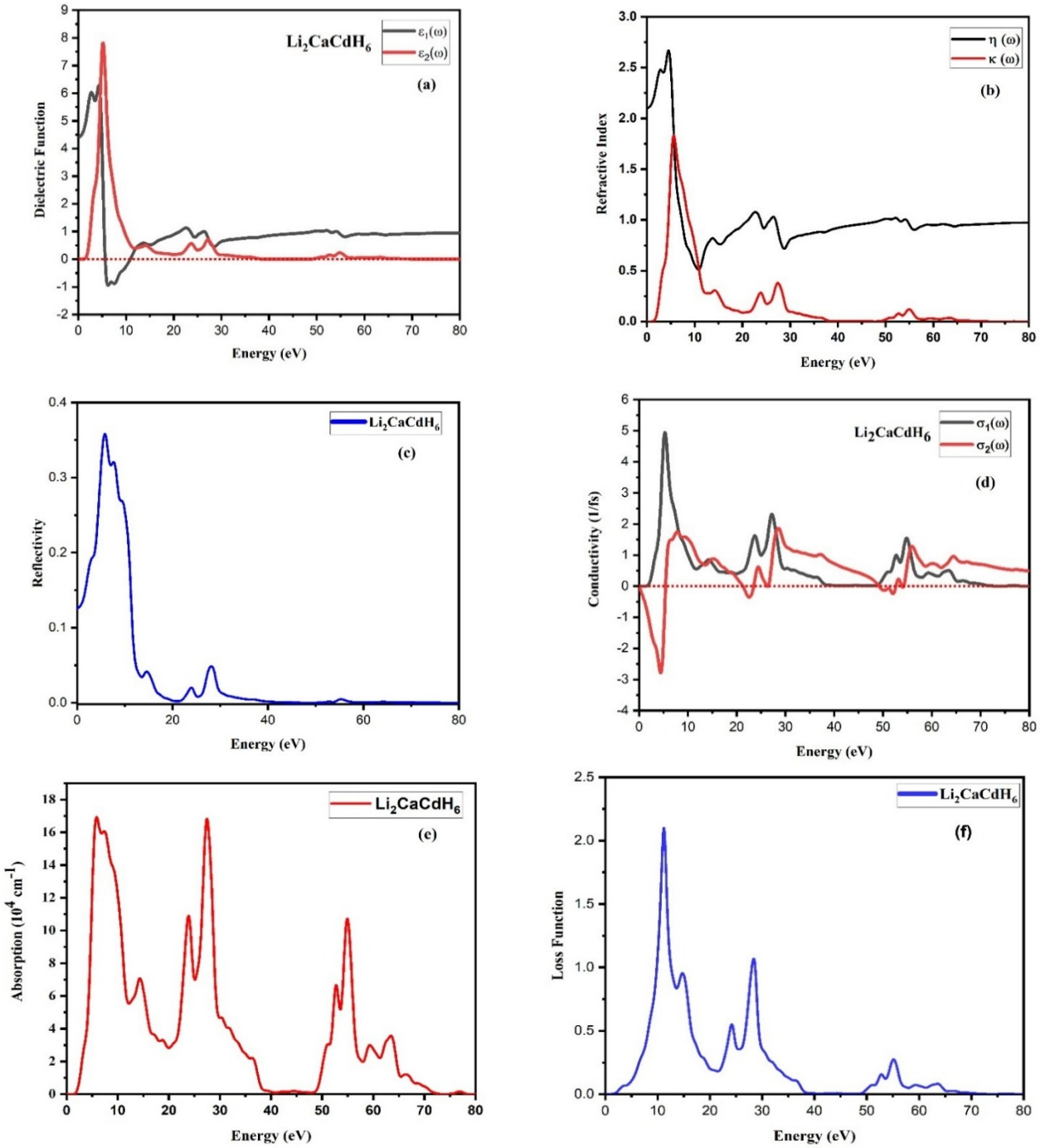

Figure 5. Optical properties of Li_2CaCdH_6 (a) dielectric function, (b) refractive index, (c) reflectivity, (d) conductivity, (e) absorption, and (f) loss function

4. Conclusions

Perovskite, especially hydride materials, has emerged as a focal point in renewable and green energy systems, particularly for their role in H_2-storage. Using the DFT technique, the structural, optical, mechanical, electrical, and hydrogen storage properties of Li_2CaCdH_6 were thoroughly investigated. Structurally, Li_2CaCdH_6 crystallizes in space group 225 (Fm-3m), with optimized lattice constant and volume (V) of 8.27 Å and 565.85 Å^3, respectively. The gravimetric hydrogen storage capacity of Li_2CaCdH_6 was calculated to be an impressive 3.51 wt.%. Electronic band structure and density of states (DOS) analyses revealed a semiconductor nature, characterized by a band gap of 1.95 eV, while structural stability was confirmed by a negative formation enthalpy of -2.65 eV/atom. Mechanical properties were also explored, with elastic constants (C_{11} = 46.995, C_{12} = 23.879, C_{44} = 8.641 GPa), modulus values (B = 31.585, Y = 26.665, G = 9.808 GPa), Pugh's ratio of 3.22, Poisson's ratio (ν = 0.36), and anisotropy factor (A = 4.07) calculated for Li_2CaCdH_6. Material shows Ductile behavior. The Cauchy's pressure (C_p = 15.24) and Born stability criteria validated the mechanical stability. The highest absorption for the compound in the ultraviolet region reaches 169,247.33 cm^{-1} at 5.89 eV, which indicates the potential for photochemical activation of hydrogen storage processes. These findings reveal the propensity of Li_2CaCdH_6 perovskite as a promising candidate for hydrogen storage applications, offering a blend of structural integrity, electronic properties, and mechanical stability essential for advancing green energy technologies. Additionally, further efforts can focus on lowering the desorption temperature to enhance performance and feasibility.

Conflict of Interest

The author declares no conflict of interest related to the publication of this research.

Data Availability Statement

The data supporting the findings of this study are available within the article. Additional data related to the computational calculations are available from the corresponding author upon reasonable request.

Acknowledgments

The authors extend their gratitude to Govt. Postgraduate College Kohat for their support and the Higher Education Department for their assistance and resources.

Author Contributions

Investigation; Conceptualization; Software; Writing- Original Draft Preparation, S.Z.U.; Validation, Formal Analysis, D.R. and U.F.; Visualization, S.A.K. and M.u.R; Writing- Review & Editing, S.Z.U., I.S., A.J., J.R. and M.K.; Supervision, U.F. All authors have read and agreed to the published version of the manuscript.

References

[1] J. Y. Lee, A. Ramasamy, K. H. Ong, R. Verayiah, H. Mokhlis, and M. Marsadek, "Energy storage systems: A review of its progress and outlook, potential benefits, barriers and solutions within the Malaysian distribution network," Journal of Energy Storage, vol. 72, pp. 108360, 2023. https://doi.org/10.1016/j.est.2023.108360

[2] J. K. Bairwa, P. K. Kamlesh, U. Rani, R. Singh, R. Gupta, S. Kumari, T. Kumar, and A. S. Verma, "Highly efficient and stable Ra2LaNbO6 double perovskite for energy conversion device applications," Materials Science for Energy Technologies, vol. 7, pp. 61-72, 2024. https://doi.org/10.1016/j.mset.2023.07.005

[3] J. K. Bairwa, M. Rani, P. K. Kamlesh, R. Singh, U. Rani, S. Al-Qaisi, T. Kumar, S. Kumari, and A. S. Verma, "Modeling and simulation of multifaceted properties of X2NaIO6 (X= Ca and Sr) double perovskite oxides for advanced technological applications," Journal of Molecular Modeling, vol. 29, no. 12, pp. 379, 2023. https://doi.org/10.1007/s00894-023-05786-z

[4] C. Tarhan, and M. A. Çil, "A study on hydrogen, the clean energy of the future: Hydrogen storage methods," Journal of Energy Storage, vol. 40, pp. 102676, 2021. https://doi.org/10.1016/j.est.2021.102676

[5] H. Yu, and C. Hebling, "Fuel Cells: Microsystems," Encyclopedia of Materials: Science and Technology, K. H. J. Buschow, R. W. Cahn, M. C. Flemings, B. Ilschner, E. J. Kramer, S. Mahajan and P. Veyssière, eds., pp. 1-13, Oxford: Elsevier, 2005.

[6] A. Franco, and C. J. H. Giovannini, "Hydrogen gas compression for efficient storage: balancing energy and increasing density," vol. 5, no. 2, pp. 293-311, 2024. https://doi.org/10.3390/hydrogen5020017

[7] M. Alenezi, B. Alarbeed, and Y. J. K. P. Alqaheem, "Metal hydrides and metal-organic frameworks for hydrogen storage in automotive applications: a review," vol. 22, no. 1, pp. 76-94, 2024. https://doi.org/10.32737/2221-8688-2024-1-76-94

[8] V. Balaji, and A. J. H. Xavior, "Development of high entropy alloys (HEAs): Current trends," vol. 10, no. 7, 2024. https://doi.org/10.1016/j.heliyon.2024.e26464

[9] E. Pomerantseva, F. Bonaccorso, X. Feng, Y. Cui, and Y. Gogotsi, "Energy storage: The future enabled by nanomaterials," Science, vol. 366, no. 6468, pp. eaan8285, 2019. https://doi.org/10.1126/science.aan8285

[10] Q. Zhang, E. Uchaker, S. L. Candelaria, and G. Cao, "Nanomaterials for energy conversion and storage," Chemical Society Reviews, vol. 42, no. 7, pp. 3127-3171, 2013. https://doi.org/10.1039/c3cs00009e

[11] S. Abdimomyn, S. Malik, M. Skakov, Y. Koyanbayev, A. Miniyazov, and F. Malchik, "Hydrogen storage materials: Promising materials for Kazakhstan's hydrogen storage industry," Eurasian Chemico-Technological Journal, vol. 26, no. 3, pp. 113-132, 2024. https://doi.org/10.18321/ectj1635

[12] M. K. Shahzad, S. Hussain, M. N. Khan, M. J. Aslam, R. M. Mohammed, V. Tirth, H. Alqahtani, A. Algahtani, T. Al-Mughanam, and W. Azeem, "Computational insights of double perovskite Na2CaCdH6 hydride alloy for hydrogen storage applications: a DFT investigation," Scientific Reports, vol. 14, no. 1, pp. 25102, 2024. https://doi.org/10.1038/s41598-024-76062-0

[13] M.-H. Kuo, N. Neykova, and I. Stachiv, "Overview of the Recent Findings in the Perovskite-Type Structures Used for Solar Cells and Hydrogen Storage," Energies, vol. 17, no. 18, pp. 4755, 2024. https://doi.org/10.3390/en17184755

[14] H. Benaali, S. Bahhar, A. Tahiri, Y. Didi, H. Fatihi, A. Abbassi, B. Manaut, and M. Naji, "Investigation of KMnH3 and KFeH3 perovskite hydrides via ab-initio for hydrogen storage," Inorganic Chemistry Communications, pp. 113033, 2024. https://doi.org/10.1016/j.inoche.2024.113033

[15] M. K. Masood, W. Khan, K. Chaoui, Z. Ashraf, S. Bibi, A. Kanwal, A. A. Alothman, and J. Rehman, "Theoretical investigation of XSnH3 (X: Rb, Cs, and Fr) perovskite hydrides for hydrogen storage application," International Journal of Hydrogen Energy, vol. 63, pp. 1248-1257, 2024. https://doi.org/10.1016/j.ijhydene.2024.03.229

[16] Z. ur Rehman, M. A. Rehman, B. Rehman, M. Amjad, M. Awais, I. Iqbal, and A. Rafique, "A DFT study of structural, electronic, mechanical, phonon, thermodynamic, and H2 storage properties of lead-free perovskite hydride MgXH3 (X= Cr, Fe, Mn)," Journal of Physics and Chemistry of Solids, vol. 186, pp. 111801, 2024. https://doi.org/10.1016/j.jpcs.2023.111801

[17] M. A. Lahlou Nabil, N. Fenineche, I. Popa, and J. J. Sunyol, "Morphological, structural and hydrogen storage properties of LaCrO3 perovskite-type oxides," Energies, vol. 15, no. 4, pp. 1463, 2022. https://doi.org/10.3390/en15041463

[18] A. R. Paul, S. Mehla, and S. Bhargava, "Intermetallic compounds for hydrogen storage: Current status and future perspectives," Small, vol. 21, no. 14, pp. 2408889, 2025. https://doi.org/10.1002/smll.202408889

[19] S. Srivastava, "Hydrogen storage materials for vehicular applications," Energy Storage, vol. 6, no. 1, pp. e524, 2024. https://doi.org/10.1002/est2.524

[20] A. Jaiswal, and S. Sahu, "Hydrogen Storage Challenge in the Hydrogen-Based Civilization," Hydrogen Fuel Cell Technology for Mobile Applications, pp. 157-181: IGI Global, 2023. https://doi.org/10.4018/978-1-6684-6721-3.ch007

[21] R. C. Muduli, and P. Kale, "Advanced materials for solid-state hydrogen storage: A review on high-surface-area innovations," International Journal of Hydrogen Energy, vol. 170, pp. 151049, 2025/09/22/, 2025. https://doi.org/10.1016/j.ijhydene.2025.151049

[22] M. Ali, Z. Bibi, M. Mubashir, M. Younis, U. Afzal, and A. El-marghany, "A computational investigation of lithium-based metal hydrides for advanced solid-state hydrogen storage," ChemistrySelect, vol. 9, no. 10, pp. e202304582, 2024. https://doi.org/10.1002/slct.202304582

[23] Q. Yin, G. Bi, R. Wang, Z. Zhao, and K. Ma, "High-capacity hydrogen storage in lithium decorated penta-BN2: A first-principles study," Journal of Power Sources, vol. 591, pp. 233814, 2024. https://doi.org/10.1016/j.jpowsour.2023.233814

[24] Z. Tang, J. Chen, Y. Xu, Z. Li, L. Sheng, Y. Hu, X. Wang, J. Wang, Y. Tang, and X. He, "Lithium-Induced Covalent Organic Frameworks with Enhanced Sorption Heat for Efficient Hydrogen Storage," Chemistry of Materials, vol. 36, no. 9, pp. 4437-4443, 2024. https://doi.org/10.1021/acs.chemmater.4c00059

[25] W. Khan, M. K. Masood, K. Chaoui, R. Sharma, N. Ashraf, R. Rafique, A. Hammad, A. A. Alothman, and J. Rehman, "First-principles analysis of physical properties of the novel calcium-based hydrides for hydrogen storage application," Physics Letters A, vol. 504, pp. 129443, 2024. https://doi.org/10.1016/j.physleta.2024.129443

[26] J. Kim, H. Kim, J. Kim, H. Bae, A. Singh, T. Hussain, and H. Lee, "Calcium-decorated polygon-graphenes for hydrogen storage," ACS Applied Energy Materials, vol. 6, no. 12, pp. 6807-6813, 2023. https://doi.org/10.1021/acsaem.3c01020

[27] M. A. Alheety, S. N. Ismail, E. M. Ali, and A. M. A. Hussien, "Cadmium oxide: green synthesis, characterization and H 2 storage performance," Authorea Preprints, vol. 1, pp. 1-5, 2023. https://doi.org/10.22541/au.169232049.90866351/v1

[28] W. Li, and C. Wang, "Development of Highly Efficient CdS-Based Photocatalysts for Hydrogen Production: Structural Modification, Durability, and Mechanism," UV-Visible Photocatalysis for Clean Energy Production and Pollution Remediation: Materials, Reaction Mechanisms, and Applications, pp. 153-169, 2023. https://doi.org/10.1002/9783527837991.ch11

[29] W. Azeem, S. Hussain, M. K. Shahzad, F. Azad, G. Khan, V. Tirth, H. Alqahtani, A. Algahtani, T. Al-Mughanam, and Y. H. Wong, "Computational insights of double perovskite X2CaCdH6 (X= Rb and Cs) hydride materials for hydrogen storage applications: A DFT analysis," International Journal of Hydrogen Energy, vol. 79, pp. 514-524, 2024. https://doi.org/10.1016/j.ijhydene.2024.07.044

[30] S. J. Clark, M. D. Segall, C. J. Pickard, P. J. Hasnip, M. I. Probert, K. Refson, and M. C. Payne, "First principles methods using CASTEP," Zeitschrift für kristallographie-crystalline materials, vol. 220, no. 5-6, pp. 567-570, 2005. https://doi.org/10.1524/zkri.220.5.567.65075

[31] M. Segall, P. J. Lindan, M. a. Probert, C. J. Pickard, P. J. Hasnip, S. Clark, and M. Payne, "First-principles simulation: ideas, illustrations and the CASTEPcode," Journal of physics: condensed matter, vol. 14, no. 11, pp. 2717, 2002. https://doi.org/10.1088/0953-8984/14/11/301

[32] C. Adamo, and V. Barone, "Physically motivated density functionals with improved performances: The modified Perdew-Burke-Ernzerhof model," The Journal of chemical physics, vol. 116, no. 14, pp. 5933-5940, 2002. https://doi.org/10.1063/1.1458927

[33] J. P. Perdew, K. Burke, and Y. Wang, "Generalized gradient approximation for the exchange-correlation hole of a many-electron system," Physical review B, vol. 54, no. 23, pp. 16533, 1996. https://doi.org/10.1103/PhysRevB.54.16533

[34] M. Ernzerhof, and G. E. Scuseria, "Assessment of the Perdew-Burke-Ernzerhof exchange-correlation functional," The Journal of chemical physics, vol. 110, no. 11, pp. 5029-5036, 1999. https://doi.org/10.1063/1.478401

[35] M. Rani, P. K. Kamlesh, S. Kumawat, U. Rani, G. Arora, and A. S. Verma, "Rare earth-based oxides double perovskites A2NiMnO6 (A= La and Gd): applications in magneto-caloric, photo-catalytic and thermoelectric devices," Physica B: Condensed Matter, vol. 680, pp. 415645, 2024. https://doi.org/10.1016/j.physb.2023.415645

[36] M. Torrent, N. Holzwarth, F. Jollet, D. Harris, N. Lepley, and X. Xu, "Electronic structure packages: Two implementations of the projector augmented wave (PAW) formalism," Computer Physics Communications, vol. 181, no. 11, pp. 1862-1867, 2010. https://doi.org/10.1016/j.cpc.2010.07.036

[37] A. Dal Corso, "Projector augmented-wave method: Application to relativistic spin-density functional theory," Physical Review B-Condensed Matter and Materials Physics, vol. 82, no. 7, pp. 075116, 2010. https://doi.org/10.1103/PhysRevB.82.075116

[38] Y. Wang, Wisesa, P., Balasubramanian, A., Dwaraknath, S., & Mueller, T. , "Rapid generation of optimal generalized Monkhorst-Pack grids," Computational Materials Science, vol. 187, pp. 110100., 2021. https://doi.org/10.1016/j.commatsci.2020.110100

[39] W. S. Morgan, J. J. Jorgensen, B. C. Hess, and G. L. W. Hart, "Efficiency of Generalized Regular k-point grids," Computational Materials Science, vol. 153, pp. 424-430, 2018/10/01/, 2018. https://doi.org/10.1016/j.commatsci.2018.06.031

[40] G. Kresse, and D. Joubert, "From ultrasoft pseudopotentials to the projector augmented-wave method," Physical review b, vol. 59, no. 3, pp. 1758, 1999. https://doi.org/10.1103/PhysRevB.59.1758

[41] J. D. Head, and M. C. Zerner, "A Broyden-Fletcher-Goldfarb-Shanno optimization procedure for molecular geometries," Chemical physics letters, vol. 122, no. 3, pp. 264-270, 1985. https://doi.org/10.1016/0009-2614(85)80574-1

[42] C. Gatti, and P. Macchi, "A guided tour through modern charge density analysis," Modern Charge-Density Analysis, pp. 1-78: Springer, 2011. https://doi.org/10.1007/978-90-481-3836-4_1

[43] M. Jamal, S. J. Asadabadi, I. Ahmad, and H. R. Aliabad, "Elastic constants of cubic crystals," Computational Materials Science, vol. 95, pp. 592-599, 2014. https://doi.org/10.1016/j.commatsci.2014.08.027

[44] W. Voigt, and W. Voigt, Wechselbeziehungen zwischen zwei Tensortripeln.(Elastizität und innere Reibung.): Springer, 1966. https://doi.org/10.1007/978-3-663-15884-4_8

[45] R. S. Crosson, and J. W. Lin, "Voigt and Reuss prediction of anisotropic elasticity of dunite," Journal of Geophysical Research, vol. 76, no. 2, pp. 570-578, 1971. https://doi.org/10.1029/JB076i002p00570

[46] R. Hill, "The elastic behaviour of a crystalline aggregate," Proceedings of the Physical Society. Section A, vol. 65, no. 5, pp. 349, 1952. https://doi.org/10.1088/0370-1298/65/5/307

[47] T. Zelai, "Study of magnetic, thermoelectric, and mechanical properties of double perovskites Be2XH6 (X= Cr and Mn) for spintronic and hydrogen-storage applications," Inorganic Chemistry Communications, vol. 165, pp. 112579, 2024. https://doi.org/10.1016/j.inoche.2024.112579

[48] Y. Song, M. K. Shahzad, S. Hussain, A. Farrukh, M. Riaz, H. Sattar, G. Khan, G. A. Ashraf, S. M. Ali, and M. Alam, "Theoretical prediction of perovskite ARH3 (A= K, Li, Rb; RCa, Sr) hydride materials for hydrogen storage applications: A DFT investigation," International Journal of Hydrogen Energy, vol. 79, pp. 1472-1482, 2024. https://doi.org/10.1016/j.ijhydene.2024.07.069

[49] K. Cousins, and R. Zhang, "Highly Porous Organic Polymers for Hydrogen Fuel Storage," Polymers, vol. 11, no. 4, pp. 690, 2019. https://doi.org/10.3390/polym11040690

[50] C. Li, P. Peng, D. W. Zhou, and L. Wan, "Research progress in LiBH4 for hydrogen storage: A review," International Journal of Hydrogen Energy, vol. 36, no. 22, pp. 14512-14526, 2011/11/01/, 2011. https://doi.org/10.1016/j.ijhydene.2011.08.030

[51] S. Al, "Mechanical and electronic properties of perovskite hydrides LiCaH 3 and NaCaH 3 for hydrogen storage applications," The European Physical Journal B, vol. 94, no. 9, pp. 182, 2021. https://doi.org/10.1140/epjb/s10051-021-00195-8

[52] T. Tang, and Y. Tang, "Lithium doping in Na-based double perovskite for hydrogen storage and improving their optoelectrronic properties: First-principles investigation," Materials Chemistry and Physics, vol. 316, pp. 129099, 2024. https://doi.org/10.1016/j.matchemphys.2024.129099

[53] B. Ahmed, M. B. Tahir, A. Ali, and M. Sagir, "DFT insights on structural, electronic, optical and mechanical properties of double perovskites X2FeH6 (X= Ca and Sr) for hydrogen-storage applications," International Journal of Hydrogen Energy, vol. 50, pp. 316-323, 2024. https://doi.org/10.1016/j.ijhydene.2023.10.237

[54] H. H. Raza, G. Murtaza, N. Muhammad, and S. M. Ramay, "First-principle investigation of XSrH3 (X= K and Rb) perovskite-type hydrides for hydrogen storage," International Journal of Quantum Chemistry, vol. 120, no. 24, pp. e26419, 2020. https://doi.org/10.1002/qua.26419

[55] T. C.-J. Yang, P. Fiala, Q. Jeangros, and C. Ballif, "High-bandgap perovskite materials for multijunction solar cells," Joule, vol. 2, no. 8, pp. 1421-1436, 2018. https://doi.org/10.1016/j.joule.2018.05.008

[56] M. Born, "On the stability of crystal lattices. I." pp. 160-172. https://doi.org/10.1017/S0305004100017138

[57] F. Mouhat, and F.-X. Coudert, "Necessary and sufficient elastic stability conditions in various crystal systems," Physical review B, vol. 90, no. 22, pp. 224104, 2014. https://doi.org/10.1103/PhysRevB.90.224104

[58] R. Gaillac, P. Pullumbi, and F.-X. Coudert, "ELATE: an open-source online application for analysis and visualization of elastic tensors," Journal of Physics: Condensed Matter, vol. 28, no. 27, pp. 275201, 2016. https://doi.org/10.1088/0953-8984/28/27/275201

[59] A. Ayyaz, S. Saidi, N. D. Alkhaldi, G. Murtaza, N. Sfina, and Q. Mahmood, "Lead-free double perovskites Rb2TlSbX6 (X= Cl, Br, and I) as an emerging aspirant for solar cells and green energy applications," Solar Energy, vol. 279, pp. 112844, 2024. https://doi.org/10.1016/j.solener.2024.112844

[60] D. Behera, A. Dixit, A. Azzouz-Rached, A. Bentouaf, M. F. Rahman, H. Albalawi, A. Bouhenna, E. S. Yousef, and R. Sharma, "Prediction of new MAX phase Zr2MSiC2 (M= Ti, V) compounds as a promising candidate for future engineering: DFT calculations," Materials Science and Engineering: B, vol. 301, pp. 117141, 2024. https://doi.org/10.1016/j.mseb.2023.117141

[61] M. Radjai, S. S. Essaoud, A. Bouhemadou, D. Allali, A. Bedjaoui, S. Bin-Omran, R. Khenata, and Y. Al-Douri, "Computational investigation of the structural, elastic, electronic, and thermodynamic properties of chloroperovskites GaXCl3 (X= Be, Ca, or Sr) using DFT framework," Physica Scripta, vol. 99, no. 6, pp. 065917, 2024. https://doi.org/10.1088/1402-4896/ad418b

[62] M. Sanati, R. Albers, T. Lookman, and A. Saxena, "Elastic constants, phonon density of states, and thermal properties of UO 2," Physical Review B-Condensed Matter and Materials Physics, vol. 84, no. 1, pp. 014116, 2011. https://doi.org/10.1103/PhysRevB.84.014116

[63] M. Eldlio, F. Che, and M. Cada, "Drude-Lorentz model of semiconductor optical plasmons." pp. 41-49. https://doi.org/10.1007/978-94-007-6818-5_4

[64] M. Abd El-Raheem, M. R. Ahmed, and S. A. Mohamed, "Influence of the rate of flow of argon on the optical properties of the MnSmO3 films prepared by magnetron sputtering technique," Journal of Materials Science: Materials in Electronics, vol. 35, no. 17, pp. 1161, 2024. https://doi.org/10.1007/s10854-024-12737-8

[65] A. Erraji, R. Masrour, and L. Xu, "Investigation of electrochemical, structural, electronic, thermodynamic, and optical properties of LiTi2O4 cathode material for Li-ion battery: an Ab Initio calculations," Ionics, vol. 30, no. 10, pp. 5979-5987, 2024. https://doi.org/10.1007/s11581-024-05744-6

[66] F. A. Nelson, A. Basem, D. J. Jasim, T. E. Gber, M. T. Odey, A. F. Al Asmari, and S. Islam, "Chemical effect of alkaline-earth metals (Be, Mg, Ca) substitution of BFe2XH hydride perovskites for applications as hydrogen storage materials: A DFT perspective," International Journal of Hydrogen Energy, vol. 79, pp. 1191-1200, 2024. https://doi.org/10.1016/j.ijhydene.2024.07.063

[67] O. Stenzel, "The Kramers-Kronig Relations," The Physics of Thin Film Optical Spectra: An Introduction, pp. 83-90: Springer, 2024. https://doi.org/10.1007/978-3-031-65030-7_5

[68] S. Zhu, T. P. Chen, Z. H. Cen, E. S. M. Goh, S. F. Yu, Y. C. Liu, and Y. Liu, "Split of surface plasmon resonance of gold nanoparticles on silicon substrate: a study of dielectric functions," Optics Express, vol. 18, no. 21, pp. 21926-21931, 2010/10/11, 2010. https://doi.org/10.1364/OE.18.021926

[69] Y. Sun, and K. F. Aguey-Zinsou, "Light-Activated Hydrogen Storage in Mg, LiH and NaAlH4," ChemPlusChem, vol. 83, no. 10, pp. 904-908, 2018. https://doi.org/10.1002/cplu.201800190